

Cite this: *Mater. Adv.*, 2022,  
3, 8922Received 3rd October 2022,  
Accepted 16th October 2022

DOI: 10.1039/d2ma00949h

rsc.li/materials-advances

## Crystallized glass tailored by controlled heat treatment for carbon dioxide capture under mild conditions†

Hyung-Ju Kim,<sup>a</sup> Hee-Chul Yang,<sup>a</sup> Keunyoung Lee<sup>a</sup> and  
Richard I. Foster<sup>\*ab</sup>

Described is the formation of crystallized alkaline earth oxide-containing glass adsorbents for radioactive carbon dioxide ( $^{14}\text{CO}_2$ ) sequestering and mineralization under mild operating conditions; thus enabling the long-term geological disposal of hazardous  $^{14}\text{C}$ . The best performing crystallized glass adsorbents recorded a max  $\text{CO}_2$  capacity of  $4.54 \text{ mmol g}^{-1}$  and a carbonation reaction rate of  $8.04 \text{ mmol g}^{-1} \text{ h}^{-1}$ .

Radioactive carbon dioxide ( $^{14}\text{CO}_2$ ) capture using innovative materials is desirable due to associated radiological hazards,<sup>1</sup> and growing climate change.<sup>2,3</sup> In recent years, modified activated carbons,<sup>4</sup> metal-organic frameworks,<sup>5,6</sup> modified 3D graphene,<sup>7</sup> covalent organic frameworks,<sup>8</sup> and natural minerals<sup>9</sup> have been considered as adsorbents for  $\text{CO}_2$ . Mineral carbonation technology (MCT) is amenable to irreversibly capture  $\text{CO}_2$ , for example in the form of natural minerals,<sup>9,10</sup> or their mimics.<sup>11,12</sup> Typically, MCT is attractive because capturing carbon through the chemical reaction between alkaline earth metal ions and  $\text{CO}_2$  forms insoluble and significantly stable carbonates.<sup>13</sup> However, most applications of MCT have an intrinsic restriction regarding their operational conditions since no forward reaction occurs within realistic time scales.<sup>14</sup> Thereby, the  $\text{CO}_2$  capture performance, such as  $\text{CO}_2$  capacity and carbonation reaction rate, of MCTs and their applications are severely restricted by the difficulty of operation under mild conditions. For example, natural minerals require aggressive carbonation reaction conditions *e.g.* high pressure ( $\geq 20$  bar), high temperature ( $> 373$  K), and pH-adjusted carrier solutions.<sup>15</sup> To overcome such obstacles, the fabrication of alkaline earth oxides impregnated into an amorphous glass structure

have been recently developed.<sup>16</sup> They show enhanced rates of dissolution of alkaline earth metal ions and carbonation reaction due to the loosely packed glass structure and the generation of a surface coating silica gel, consequently facilitating  $\text{CO}_2$  capture under mild conditions.<sup>16</sup>

Here, we report the synthesis and application of a crystallized glass tailored by controlled heat treatment for  $\text{CO}_2$  capture under mild conditions. The controlled heat treatment of an alkaline earth oxide-containing glass gives rise to a structural transformation from amorphous to crystalline. The structural characterizations and  $\text{CO}_2$  capture performance, including  $\text{CO}_2$  capacity, carbonation reaction rate, and the dissolution rate of alkaline earth metal ion, were analyzed to reveal the impact of controlled heat treatment and phase transformation.

The materials used, fabrication procedures for amorphous glass, its crystallization, characterization, and  $\text{CO}_2$  capacity measurement are described in detail in the ESI† (I. Materials and methods). An amorphous glass can be converted into the crystalline phase when heat-treated above its crystallization temperature, as demonstrated in Fig. S1 (ESI†). This crystallized glass is often referred to as glass-ceramic.<sup>17</sup> As shown in Fig. 1, the X-ray diffraction (XRD) pattern of the crystallized Sr-glass- $\text{Na}_2\text{O}$ , prior to  $\text{CO}_2$  capture, showed crystallinity including strontium oxide. These crystalline peaks were indexed as strontium metaborate (Joint Committee on Powder Diffraction Standards (JCPDS),  $\text{SrB}_2\text{O}_4$ ; No. 15-0779). This definitive structure was previously reported as orthorhombic symmetry and *Pbcn* space group with  $a = 12.0135$ ,  $b = 4.339$ , and  $c = 6.5864 \text{ \AA}$ .<sup>18,19</sup> After  $\text{CO}_2$  capture, the structure of  $\text{SrB}_2\text{O}_4$  was completely converted into the structure of  $\text{SrCO}_3$  (JCPDS, No. 05-0418), which coincides well with the pattern in Fig. 1 without any remaining peaks from  $\text{SrB}_2\text{O}_4$ . That is to say, the crystallized Sr-glass- $\text{Na}_2\text{O}$  reacted with  $\text{CO}_2$  in the aqueous phase to form carbonates, and  $\text{SrB}_2\text{O}_4$  is fully converted to  $\text{SrCO}_3$ .

The Fourier transform infrared attenuated total reflectance (FT-IR/ATR) spectroscopy of the  $45 \mu\text{m}$ -sized crystallized Sr-glass- $\text{Na}_2\text{O}$

<sup>a</sup> Decommissioning Technology Research Division, Korea Atomic Energy Research Institute, 989-111 Daedeok-daero, Yuseong-gu, Daejeon 34057, Republic of Korea. E-mail: hyungjukim@kaeri.re.kr

<sup>b</sup> Nuclear Research Institute for Future Technology and Policy, Seoul National University, 1 Gwanak-ro, Gwanak-gu, Seoul 08826, Republic of Korea. E-mail: rifoster@snu.ac.kr

† Electronic supplementary information (ESI) available: Materials and methods, supporting figures, table. See DOI: <https://doi.org/10.1039/d2ma00949h>



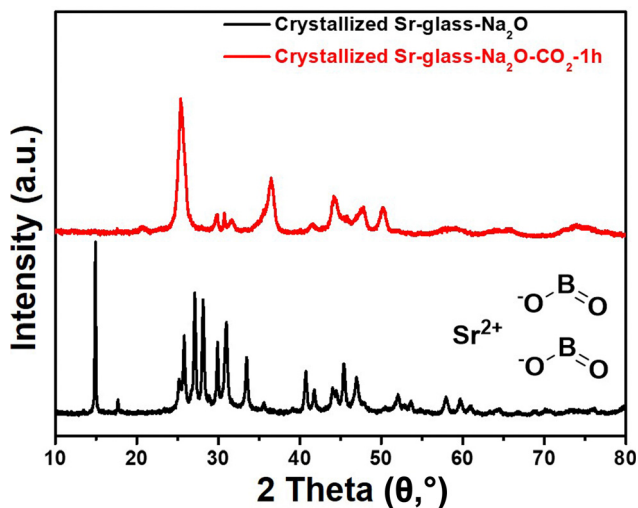


Fig. 1 XRD patterns of the crystallized Sr-glass- $\text{Na}_2\text{O}$  (45  $\mu\text{m}$ ) prior and subsequent to 1 h of  $\text{CO}_2$  capture at 298 K.

prior and subsequent to 1 h of  $\text{CO}_2$  capture at 298 K was characterized as shown in Fig. 2a. The peaks near  $1450\text{ cm}^{-1}$  (stretching vibration) and  $850\text{ cm}^{-1}$  (bending vibration) visibly appear after  $\text{CO}_2$  capture. The presence of these peaks indicates the formation of  $\text{SrCO}_3$ ; an observation supporting the XRD patterns.<sup>20</sup> The C1s peaks near 290 eV in the X-ray photoelectron spectroscopy (XPS) intensified after 1 h of  $\text{CO}_2$  exposure as shown in Fig. 2b, further confirming the capture and subsequent formation of carbonate.<sup>21</sup> Moreover, the  $\text{N}_2$  physisorption revealed the textural properties of crystallized Sr-glass- $\text{Na}_2\text{O}$ . As shown in  $\text{N}_2$  adsorption isotherms (Fig. 3), the crystallized Sr-glass- $\text{Na}_2\text{O}$  is absolutely a nonporous material classified by International Union of Pure and Applied Chemistry Type-II adsorption isotherm.<sup>22</sup> Subsequent to 1 h of  $\text{CO}_2$  capture at 298 K, slight porosity is tailored due to the dissolved Sr from the material and newly produced  $\text{SrCO}_3$ . This is even more elucidated when the pore size distribution is analysed by Broekhoff-deBoer-Frenkel-Halsey-Hill

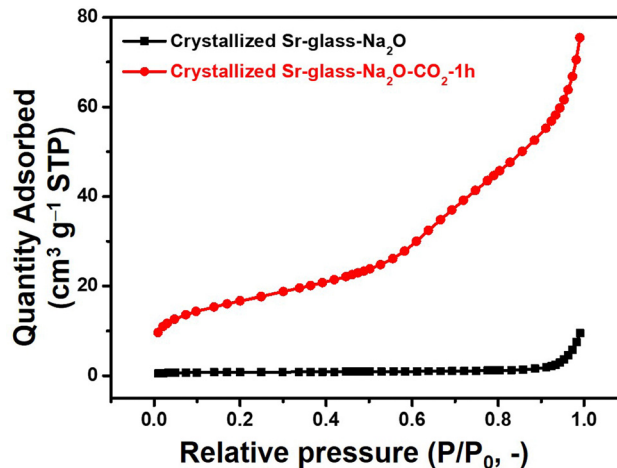


Fig. 3  $\text{N}_2$  adsorption isotherms at 77 K for crystallized Sr-glass- $\text{Na}_2\text{O}$  (45  $\mu\text{m}$ ) prior and subsequent to 1 h of  $\text{CO}_2$  capture at 298 K.

method (Fig. S2, ESI<sup>†</sup>). Relative to the nonporous crystallized Sr-glass- $\text{Na}_2\text{O}$ , the crystallized Sr-glass- $\text{Na}_2\text{O-CO}_2$  displays higher intensity in the mesopore (2–50 nm) range. The textural properties including Brunauer–Emmett–Teller (BET) surface area and pore volume are summarized in Table S1 (ESI<sup>†</sup>). Prior and subsequent to 1 h of  $\text{CO}_2$  capture, the BET surface area increases from 1.43 to  $51.13\text{ m}^2\text{ g}^{-1}$  and pore volume increases from 0.014 to  $0.117\text{ cm}^3\text{ g}^{-1}$ .

The  $\text{CO}_2$  capacities of the crystallized Sr-glass- $\text{Na}_2\text{O}$  was analyzed as a function of time. As shown in Fig. 4a, the maximum recorded  $\text{CO}_2$  capacity was  $4.54\text{ mmol g}^{-1}$  for crystallized Sr-glass- $\text{Na}_2\text{O}$  after 3 h of reaction. Notably,  $\text{CO}_2$  capacity after 12 h of reaction was exactly the same as that after 3 h based on the thermogravimetric analysis curve (Fig. S3, ESI<sup>†</sup>) which demonstrates that  $\text{CO}_2$  capture was completed within 3 h, and the carbonation reaction was under equilibrium during the rest of the time. Crystallized Sr-glass- $\text{Na}_2\text{O}$  had a higher capture efficiency (90.25%) and faster carbonation

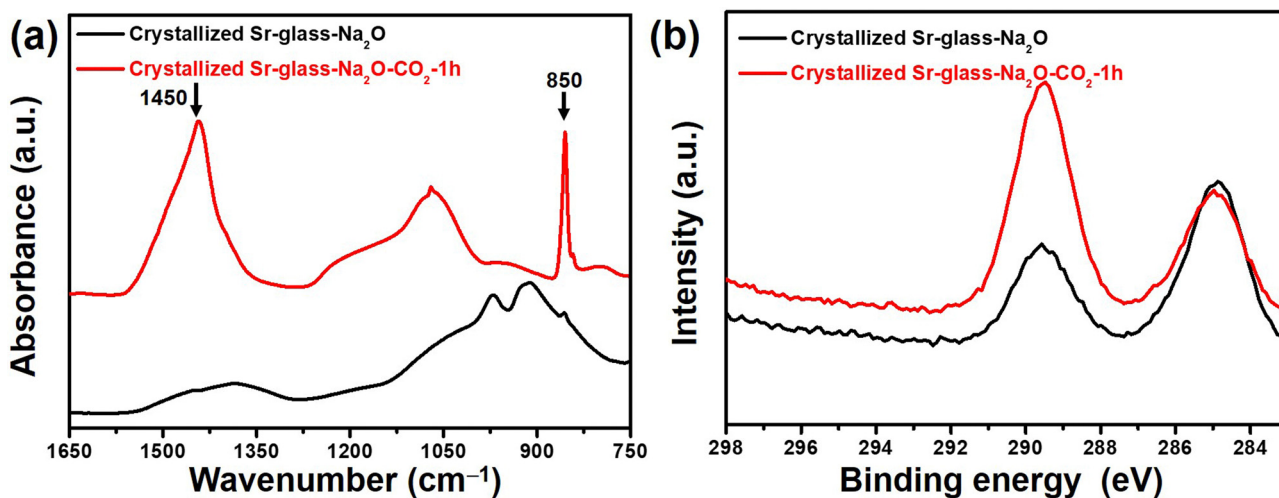


Fig. 2 (a) FT-IR/ATR absorption spectra, and (b) XPS C1s spectra of crystallized Sr-glass- $\text{Na}_2\text{O}$  (45  $\mu\text{m}$ ) prior and subsequent to 1 h of  $\text{CO}_2$  capture at 298 K.



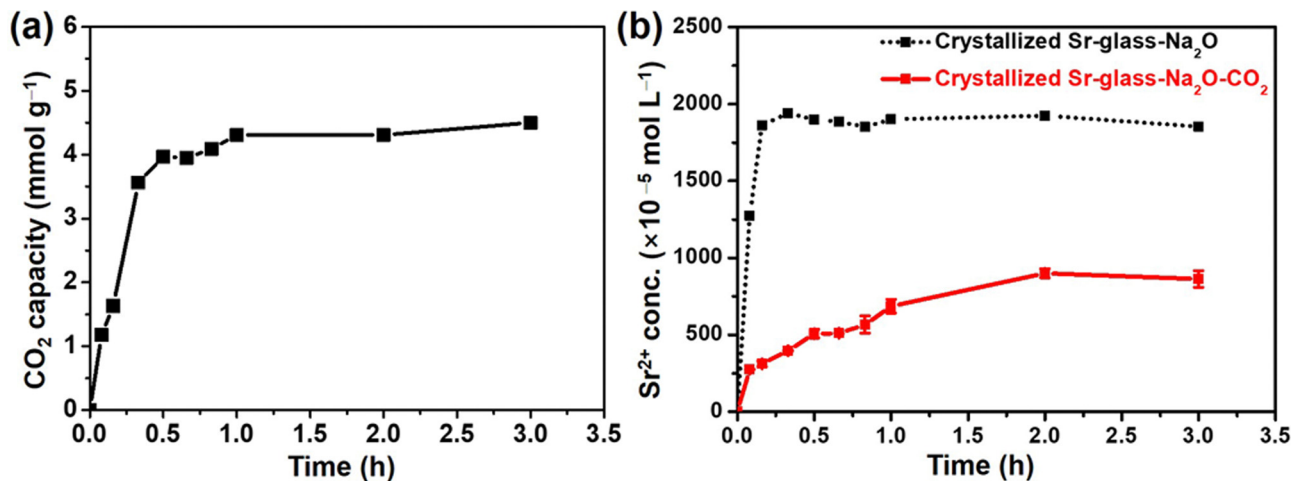


Fig. 4 (a) CO<sub>2</sub> capacity of crystallized Sr-glass-Na<sub>2</sub>O (45 μm) and (b) equivalent molar concentrations of Sr<sup>2+</sup> ion in the supernatant solutions under CO<sub>2</sub> flowing (solid black line) and CO<sub>2</sub> non-flowing (dotted red line) conditions at 298 K as a function of the reaction time.

reaction rate (8.04 mmol g<sup>-1</sup> h<sup>-1</sup> within 30 min) than our previously reported Sr-glass-Na<sub>2</sub>O (88.07% and 7.25 mmol g<sup>-1</sup> h<sup>-1</sup>).<sup>16</sup> Efficiency calculations were performed as a ratio of the experimental and theoretical CO<sub>2</sub> capacities [experimental CO<sub>2</sub> capacity/theoretical CO<sub>2</sub> capacity × 100]. This improved performance is attributed to the enhanced dissolution of Sr<sup>2+</sup> ion from the crystalline structure. Once the crystalline structure formed, most of the Sr<sup>2+</sup> ions were present in the crystalline structure. Since most of the Sr<sup>2+</sup> ions were gathered in the crystalline phase, they easily reacted on the specific sites and converted to SrCO<sub>3</sub>. Thus, CO<sub>2</sub> capture performance was further improved comparing with amorphous Sr-glass-Na<sub>2</sub>O which had evenly distributed Sr<sup>2+</sup> ions in the structure. To further explain the observations, the Sr<sup>2+</sup> dissolution rate, which is a rate-limiting step, was studied by inductively coupled plasma-optical emission spectroscopy analyzing the molar concentration of Sr<sup>2+</sup> ions released from the crystallized glass under the conditions where CO<sub>2</sub> was either flowing or non-flowing as a function of the time (Fig. 4b). Notably, under the CO<sub>2</sub> non-flowing condition (dotted lines), crystallized Sr-glass-Na<sub>2</sub>O possessed higher solubility than that of amorphous Sr-glass-Na<sub>2</sub>O described elsewhere,<sup>16</sup> thereby almost 4 times higher

(2000 × 10<sup>-5</sup> mol L<sup>-1</sup>) saturated concentration of Sr<sup>2+</sup> ion. This coincides well with the advanced CO<sub>2</sub> capture performances (capacity, reaction rate and efficiency) of crystallized Sr-glass-Na<sub>2</sub>O. The crystallized glass also exhibited the gradual increase of ion concentrations while CO<sub>2</sub> capture showed similar tendency as those of amorphous glass adsorbent, but the reaction rate and efficiency of crystallized Sr-glass-Na<sub>2</sub>O were much higher than other glass adsorbents because of the enhanced Sr<sup>2+</sup> ion solubility in water.

The CO<sub>2</sub> capture performance, max CO<sub>2</sub> capacity in mmol g<sup>-1</sup> and CO<sub>2</sub> carbonation rate in mmol g<sup>-1</sup> h<sup>-1</sup>, of newly developed crystallized Sr-glass-Na<sub>2</sub>O was compared with those of its amorphous glass adsorbent equivalent and other natural minerals under relatively mild CO<sub>2</sub> capture conditions reported previously (Table 1). As discussed, crystallized Sr-glass-Na<sub>2</sub>O outperformed the precursor amorphous framework both in terms of CO<sub>2</sub> capacity and CO<sub>2</sub> carbonation rate with an almost doubling of performance. Even if natural minerals, such as serpentine and wollastonite, containing alkaline earth metals (Mg and Ca), exhibited a superior max CO<sub>2</sub> capacity than crystallized Sr-glass-Na<sub>2</sub>O, the aggressive CO<sub>2</sub> capture conditions (*i.e.*, energy intensive high temperature as well as acidic or

Table 1 Performance comparison of max CO<sub>2</sub> capacity and CO<sub>2</sub> carbonation rate of the crystallized Sr-glass-Na<sub>2</sub>O with other lab-made or natural adsorbents capturing CO<sub>2</sub> via mineral carbonation mechanism under relatively mild temperature and pressure (1 bar) conditions

Mineral carbonation material	Max CO <sub>2</sub> capacity [mmol g <sup>-1</sup> ]	CO <sub>2</sub> carbonation rate [mmol g <sup>-1</sup> h <sup>-1</sup> ]	Temperature [K]	Media	Ref.
Crystallized Sr-glass-Na <sub>2</sub> O	4.54	8.04 <sup>a</sup>	298	Deionized water	This work
Sr-glass-Na <sub>2</sub> O	4.43	4.09 <sup>a</sup>	298	Deionized water	16
Serpentine	7.04	7.04	343	Orthophosphoric, oxalic, and ethylenediaminetetraacetic acid	23,24
Serpentine	7.58	2.53	413	NH <sub>4</sub> HSO <sub>4</sub> /NH <sub>3</sub>	25,26
Serpentine	2.53	0.10	598	HCl/NaOH	27
Wollastonite	7	2.33	298	NH <sub>4</sub> OH	28
Wollastonite	7.95	2.65	298	NH <sub>4</sub> OH	29
Wollastonite	7.95	5.30	298	NH <sub>4</sub> Cl/HCl	30

<sup>a</sup> CO<sub>2</sub> carbonation rate was obtained from the initial 1 h of CO<sub>2</sub> capture.



basic reaction media) were required as shown in Table 1. Nonetheless, the crystallized glass adsorbent fabricated in this work showed an extremely high initial CO<sub>2</sub> carbonation rate with a decent max CO<sub>2</sub> capacity even under moderate and favourable temperature, pressure, and media, where other natural adsorbents are not able to capture CO<sub>2</sub>. For example, when the CO<sub>2</sub> capture was performed under room temperature (298 K) and atmospheric pressure (1 bar), the acidic and basic media were inevitably required to obtain a high CO<sub>2</sub> capacity for wollastonite,<sup>28–30</sup> and there was no report with such mild conditions when using serpentinite to the best of the authors' knowledge. In the crystallized Sr-glass-Na<sub>2</sub>O, alkaline earth metal ions were more easily dissolved and captured CO<sub>2</sub> in comparison with natural minerals. This suggests that the appropriate support phase, here crystallized glass, as well as the incorporation of alkaline earth oxides make the highly efficient CO<sub>2</sub> capture feasible under mild capture conditions, which is applicable to <sup>14</sup>CO<sub>2</sub> sequestration.

In conclusion, the fabrication of crystallized glass by restructuring *via* controlled heat treatment has been demonstrated; thereby implying better glass adsorbent for CO<sub>2</sub> capture than other MCT materials. The newly fabricated crystallized Sr-glass-Na<sub>2</sub>O, also called SrB<sub>2</sub>O<sub>4</sub>, exhibits even higher performance in CO<sub>2</sub> capacity, carbonation rate, and efficiency due to the enhanced dissolution of alkaline earth metal ion; in this case Sr<sup>2+</sup>. This development clearly suggests that the crystallized glass can be a technologically more desirable platform for long-term CO<sub>2</sub> capture, especially <sup>14</sup>CO<sub>2</sub> disposal and storage security.

Hyung-Ju Kim: conceptualization, methodology, validation, formal analysis, investigation, writing – original draft, writing – review & editing, visualization. Hee-Chul Yang: resources. Keunyoung Lee: project administration. Richard I. Foster: writing – reviewing and editing.

## Conflicts of interest

There are no conflicts to declare.

## Acknowledgements

This work was supported by the National Research Foundation of Korea (NRF) grant funded by the Korea government (MSIP) (No. NRF-2022M2E9A2053685).

## References

- M. Lou Dunzik-Gougar and T. E. Smith, *J. Nucl. Mater.*, 2014, **451**, 328–335.
- N. Abas and N. Khan, *J. CO<sub>2</sub> Util.*, 2014, **8**, 39–48.
- P. Bains, P. Psarras and J. Wilcox, *Prog. Energy Combust. Sci.*, 2017, **63**, 146–172.
- N. Abuelnoor, A. AlHajaj, M. Khaleel, L. F. Vega and M. R. M. Abu-Zahra, *Chemosphere*, 2021, **282**, 131111.
- Z. Zhang, Q. Ding, S. B. Peh, D. Zhao, J. Cui, X. Cui and H. Xing, *Chem. Commun.*, 2020, **56**, 7726.
- S. Shyshkanov, T. N. Nguyen, A. Chidambaram, K. C. Stylianou and P. J. Dyson, *Chem. Commun.*, 2019, **55**, 10964.
- Y. Lin, Y. Tian, H. Sun and T. Hagio, *Chemosphere*, 2021, **270**, 129420.
- Y. Huang, X. Hao, S. Ma, R. Wang and Y. Wang, *Chemosphere*, 2022, **291**, 132795.
- S. Ó. Snæbjörnsdóttir, B. Sigfússon, C. Marieni, D. Goldberg, S. R. Gislason and E. H. Oelkers, *Nat. Rev. Earth Environ.*, 2020, **1**, 90–102.
- A. Sanna, M. Uibu, G. Caramanna, R. Kuusik and M. M. Maroto-Valer, *Chem. Soc. Rev.*, 2014, **43**, 8049–8080.
- I. M. Power, A. L. Harrison and G. M. Dipple, *Environ. Sci. Technol.*, 2016, **50**, 2610–2618.
- O. Rahmani, *J. CO<sub>2</sub> Util.*, 2020, **35**, 265.
- A. A. Olajire, *J. Pet. Sci. Eng.*, 2013, **109**, 364–392.
- S. P. Veetil and M. Hitch, *Int. J. Environ. Sci. Technol.*, 2020, **17**, 4359–4380.
- S. J. Gerdemann, W. K. O'Connor, D. C. Dahlin, L. R. Penner and H. Rush, *Environ. Sci. Technol.*, 2007, **41**, 2587–2593.
- H.-J. Kim, S.-J. Kim, H.-C. Yang, H.-C. Eun, K. Lee and J.-H. Lee, *J. CO<sub>2</sub> Util.*, 2022, **61**, 102001.
- R. D. Rawlings, J. P. Wu and A. R. Boccaccini, *J. Mater. Sci.*, 2006, **41**, 733–761.
- P. D. Dernier, *Acta Cryst.*, 1969, **B25**, 1001–1003.
- J. B. Kim, K. S. Lee, I. H. Suh, J. H. Lee, J. R. Park and Y. H. Shin, *Acta Cryst.*, 1996, **C52**, 498–500.
- A. L. Vasiliu, M. V. Dinu, M. M. Zaharia, D. Peptanariu and M. Mihai, *Mater. Chem. Phys.*, 2021, **272**, 125025.
- A. V. Shchukarev and D. V. Korolkov, *Cent. Eur. J. Chem.*, 2004, **2**, 347–362.
- K. S. W. Sing, *J. Porous Mater.*, 1995, **2**, 5–8.
- A. H. A. Park and L. S. Fan, *Chem. Eng. Sci.*, 2004, **59**, 5241–5247.
- A. H. A. Park, R. Jadhav and L. S. Fan, *Can. J. Chem. Eng.*, 2003, **81**, 885–890.
- X. Wang and M. M. Maroto-Valer, *ChemSusChem*, 2011, **4**, 1291–1300.
- X. Wang and M. M. Maroto-Valer, *Fuel*, 2011, **90**, 1229–1237.
- P. C. Lin, C. W. Huang, C. T. Hsiao and H. Teng, *Environ. Sci. Technol.*, 2008, **42**, 2748–2752.
- W. Ding, L. Fu, J. Ouyang and H. Yang, *Phys. Chem. Miner.*, 2014, **41**, 489–496.
- W. Ding, H. Yang, J. Ouyang and H. Long, *RSC Adv.*, 2016, **6**, 78090–78099.
- H. Xie, F. Wang, Y. Wang, T. Liu, Y. Wu and B. Liang, *Environ. Earth Sci.*, 2018, **77**, 149.

